# Dalton Transactions

Accepted Manuscript






ROYAL SOCIETY OF CHEMISTRY

www.rsc.org/dalton

# Structural variation in Zn(II) coordination polymers built with a semi-rigid tetracarboxylate and different pyridine linkers: synthesis and selective $CO_2$ adsorption studies

**Susan Sen,[a] Subhadip Neogi,[a] Arshad Aijaz,[b] Qiang Xu*[b] and Parimal K. Bharadwaj*[a]**

*[a]Department of Chemistry, Indian Institute of Technology, Kanpur 208016, India*
*[b]National Institute of Advanced Industrial Science and Technology (AIST), Ikeda, Osaka 563-8577, Japan*

## Graphical Abstract:

The $C_{2v}$ or $C_s$ symmetry in the flexibile 3,3′,5,5′-tetracarboxydiphenylmethane ligand directs the stability and porosity of the resulting frameworks in presence of Zn(II) ion, and pyridine linkers of comparable lengths.

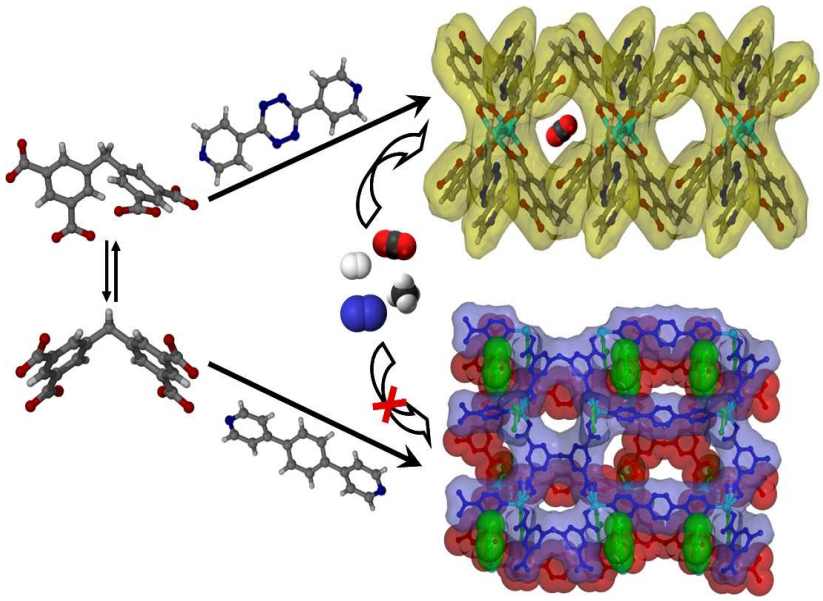

# Structural variation in Zn(II) coordination polymers built with a semi-rigid tetracarboxylate and different pyridine linkers: synthesis and selective $CO_2$ adsorption studies

**Susan Sen,[a] Subhadip Neogi,[a] Arshad Aijaz,[b] Qiang Xu*[b] and Parimal K. Bharadwaj*[a]**

## Abstract

In an effort toward rational design of porous MOFs with functionalized channel surface, 3,3′,5,5′-tetracarboxydiphenylmethane (**$H_4L_1$**) has been used in combination with two different bipyridine of similar length as linkers, and Zn(II) ions as nodes. Under solvothermal condition, two Zn(II) coordination polymers, $\{[Zn(\mathbf{H_2L_1})(\mathbf{L_2})]\cdot DMF\cdot 2H_2O\}_n$, (**1**) and $\{[Zn_2(\mathbf{L_1})(\mathbf{L_3})(DMF)_2]\cdot DMF\cdot 4H_2O\}_n$, (**2**) (DMF = dimethyl formamide, **$L_2$** = 3,6-di-pyridin-4-yl-[1,2,4,5]tetrazine, **$L_3$** =4,4′-bispyridylphenyl) are formed in moderate yields. The obvious kink in the central methylene spacer of **$H_4L_1$** induces either $C_{2v}$ or $C_s$ symmetry in the ligand, allowing different architectures of the resulting frameworks. Single crystal X-ray analysis shows that compound **1** is an one-dimensional (1D) double chain architecture with rhombus voids, linked by the $Zn_2(CO_2)_4$ paddle wheel SBUs. Tetrazine and pyridine moieties of the co-ligand and free carboxylic acid groups are lined along the voids of the framework. Compound **2**, on the other hand, crystallizes as an infinite two-dimensional corrugated sheet structure, where individual sheet is stacked in ---ABAB--- patterns along the crystallographic *b*-axis. Thermogravimetric analysis (TGA) and variable temperature powder X-ray diffraction (VTPXRD) studies reveal high thermal stability of **1**, but **2** collapses soon after desolvation. Desolvated framework **1′** shows selective $CO_2$ adsorption over $N_2$, $H_2$, and $CH_4$ at 273 K, with isosteric heat of $CO_2$ adsorption 21.3 kJ $mol^{-1}$, suggesting interaction of $CO_2$ molecules with the channel walls.

## Introduction

In recent years, functional porous metal-organic frameworks (MOFs) are emerging[1,2] as very promising materials for gas storage[3], separation[4], heterogeneous catalysis[5], sensing[6] and so on. To probe the paradigms for optimal gas adsorption, two strategies have been widely considered: functionalization of channel surfaces through introduction of proper linkers for significant interaction with gas molecules[7] with the surfaces and creation of open coordination sites on the metal in the pore wall.[8] Functionalization of the pore walls is also of immense importance to activate organic molecules to undergo heterogeneous catalysis. However, fabrication of the guest accessible functional organic sites on the pore surface is a challenging task as these groups often tend to coordinate metal ions through a self-assembly process, resulting in a framework where these functional sites may be completely blocked.[9] However, chemists have often come up with suitable strategies to overcome this problem. Incorporation of accessible nitrogen-donor sites into the pore walls of a porous material can drastically impact their gas uptake capacity and selectivity, especially for the $CO_2$ capture.[10] This event arises due to the dipole–quadrupole interactions between the polarizable mildly acidic $CO_2$ molecule and the accessible basic nitrogen donor site.[11] Based on the above annotations, we figured that introduction of nitrogen-rich tetrazine ring in the pore walls of an MOF should enhance its performance of $CO_2$ capture. Presently, selective $CO_2$ adsorption in porous frameworks has been an area of research[10,11] of utmost importance due to its environmental concerns.

The choice of the secondary building units (SBUs) is extremely important to build porous as well as robust MOFs. In many cases, these SBUs play key roles in directing the final framework topology and modulate their mechanical and physical properties significantly.[12] Apart from well known tetranuclear $Zn_4O(CO_2)_6$ SBU, dinuclear $M_2(CO_2)_4$ paddle-wheel SBUs (M = transition metal ions) are suitable to form robust MOFs and also offer two distinct coordination centers for organic ligands: one for carboxylate- and the other for pyridyl-based

linkers.[13] Assembly of these two types of organic linkers with paddle-wheel SBUs should offer better possibilities of creating additional binding sites in organic linkers that can ultimately exhibit augmented physicochemical properties.

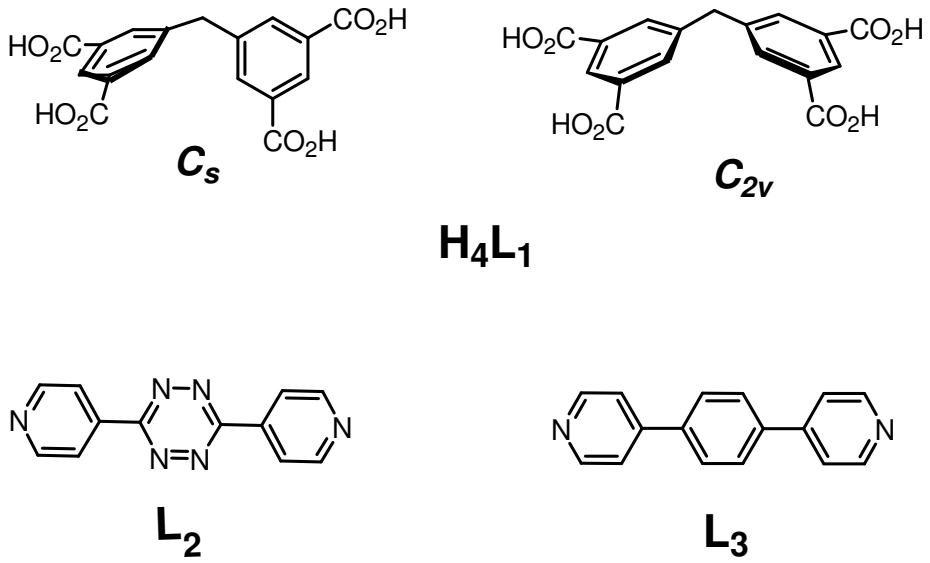


**Scheme 1** Schematic diagram of the ligands used in the present study.

With aforesaid strategies in mind, we successfully synthesized two different $Zn^{2+}$ coordination polymers based on common 3,3′,5,5′-tetracarboxydiphenylmethane ligand (**$H_4L_1$**), and two bipyridine linkers (Scheme 1) under solvothermal condition. Because of its sturdy coordination with Zn(II) ions, the tetracarboxylic acid is effective in forming robust structure. Furthermore, the obvious kink in the central methylene spacer can induce either $C_{2v}$ or $C_s$ symmetry in the ligand (Scheme 1), allowing diverse architectures of the resulting frameworks.[14] The desolvated structure, where the tetrazine and basic pyridine moieties are affixed on the pore wall, shows high thermal stability and selective $CO_2$ gas adsorption behavior over $N_2$, $H_2$ and $CH_4$ at 273 K.

## Experimental

### Materials and method

Reagent grade $Zn(NO_3)_2.6H_2O$ and 3,3',5,5'-tetracarboxydiphenylmethane (**$H_4L_1$**) were purchased from Sigma-Aldrich and used as received. Ligands **$L_2$** and **$L_3$** were prepared according to the literature procedures,[15] and their purity were monitored by NMR and elemental analyses. All solvents were purified prior to use following the established procedures.

### Physical measurements

Spectroscopic data were collected as follows: IR spectra (KBr disk, 400–4000 $cm^{-1}$) were recorded on a Perkin-Elmer Model 1320 spectrometer. Powder X-ray diffraction (PXRD) patterns were recorded on a Bruker D8 Advance diffractometer equipped with nickel-filtered $CuK_\alpha$ radiation. The tube voltage and current were 40 kV and 40 mA, respectively. Thermogravimetric analysis (TGA) (5 degree/min heating rate under nitrogen atmosphere) was performed with a Mettler Toledo Star System. $^1$H-NMR spectra were recorded on a JEOL JNM-LA500 FT instrument (500 MHz) in DMSO-$d_6$ with TMS as the internal standard. Gas adsorption measurements were performed using automatic volumetric adsorption equipments (BELSORP mini II, BEL Japan, Inc.). Prior to BET adsorption measurements, compound **1** was immersed in ethanol solvent for 3 days at room temperature to replace lattice guest molecules and after that, the complex was heated to 120 °C for 12 h under vacuum to produce the guest-free framework (**1′**).

### Synthesis of $\{[Zn(H_2L_1)(L_2)]\cdot DMF\cdot 2H_2O\}_n$, (1)

Compound **1** was synthesized by mixing 0.1 mmol of **$H_4L_1$**, 0.1 mmol of **$L_2$** and 0.4 mmol of $Zn(NO_3)_2,6H_2O$ in 3 mL of DMF in a Teflon-lined autoclave. It was heated under autogenous pressure to 90 °C for 48 h. Cooling to room temperature at a rate of 10 °C per h,

afforded the product as purple crystals in ~52% yield. Anal. calcd. for $C_{32}H_{29}N_7O_{11}Zn$: C, 51.04; H, 3.88; N, 13.02 %. Found: C, 50.87; H, 4.01; N, 12.88%.

**Synthesis of $\{[Zn_2(L_1)(L_3)(DMF)_2]\cdot DMF\cdot 4H_2O\}_n$, (2)**

This compound was synthesized in the same way as that of **1**, using $\mathbf{L_3}$ instead of $\mathbf{L_2}$. The product was isolated as pale colour crystals in ~48% yield. Anal. calcd. for $C_{42}H_{41}N_5O_{15}Zn_2$: C, 51.13; H, 4.19; N, 7.10 %. Found: C, 50.97; H, 4.31; N, 6.91%.

**X-ray structural studies**

Single crystal X-ray data were collected at 100 K on a Bruker SMART APEX CCD diffractometer using graphite-monochromated $MoK_\alpha$ radiation ($\lambda$ = 0.71069 Å). The linear absorption coefficients, scattering factors for the atoms, and the anomalous dispersion corrections were taken from International Tables for X-ray Crystallography. Data integration and reduction were processed with SAINT[16a] software. An empirical absorption correction was applied to the collected reflections with SADABS[16b] using XPREP[17c]. The structure was solved by the direct method using SHELXTL[16d] and was refined on $F^2$ by full-matrix least-squares technique using the SHELXL-97[16e] program package. The unit cell includes large region of disordered solvent molecules, which could not be modeled as discrete atomic sites. We therefore employed PLATON/SQUEEZE[17] to calculate the diffraction contribution of solvent molecules and, thereby to produce a set of solvent free diffraction intensities. Structure was then refined again using the data generated. The lattice parameters and structural data are collected in Table 1.

**Table 1** Crystal data and structure refinement for **1** and **2**

| | **1** | **2** |
|---|---|---|
| Empirical formula | $C_{29}H_{18}N_6O_8Zn$ | $C_{39}H_{34}N_4O_{10}Zn_2$ |
| Formula weight | 643.86 | 849.44 |
| Temperature | 100(1) K | 100(1) K |
| Radiation | $MoK_\alpha$ | $MoK_\alpha$ |
| Wavelength | 0.71069 Å | 0.71069 Å |
| Crystal system | Triclinic | Orthorhombic |
| Space group | *P-1* | *Pnma* |
| *a*, Å | 10.3954(6) | 18.9292(16) |
| *b*, Å | 12.7503(7) | 24.320(2) |
| *c*, Å | 14.0871(9) | 9.6354 (8) |
| $\alpha(^o)$ | 63.3380(10) | 90 |
| $\beta(^\circ)$ | 89.9780(10) | 90 |
| $\gamma(^o)$ | 86.0050(10) | 90 |
| V, $Å^3$ | 1663.58(17) | 4435.7(7) |
| Z | 2 | 4 |
| $\rho_{calc}$ g/$cm^3$ | 1.285 | 1.272 |
| $\mu$, $mm^{-1}$ | 0.791 | 1.136 |
| F(000) | 656 | 1744 |
| Independent refl. | 8238 | 5643 |
| Refl. used (I>2σ(I)) | 6182 | 3749 |
| $R_{int}$ value | 0.0310 | 0.0464 |
| Refinement method | Full-matrix least-squares on $F^2$ | Full-matrix least-squares on $F^2$ |
| GOOF | 1.037 | 1.135 |
| R indices [I>2σ(I)] | R1= 0.0469, wR2= 0.1151 | R1 = 0.0885, wR2 = 0.2840 |
| R indices (all data) | R1= 0.0696, wR2= 0.1216 | R1 = 0.1138, wR2 = 0.2833 |

## Results and discussion

Compounds **1** and **2** are synthesized solvothermally at 90 °C by reacting ligand $\mathbf{H_4L_1}$ and $Zn(NO_3)_2{\cdot}6H_2O$ with either $\mathbf{L_2}$ or $\mathbf{L_3}$ in 1:1:4 molar ratio, respectively. Once isolated, both **1** and **2** are highly stable in air, insoluble in water and in common organic solvents such as acetone, methanol, ethanol, chloroform, DMF and DMSO. Powder X-ray diffraction experiments show that major peak positions of experimental and simulated powder patterns are well-matched and verify the bulk purity. Although, we could not locate the lattice solvent molecules in both the structures, because of high disorder, their presence are pledged from TGA and matched with the free electron count from squeeze results.[17] Satisfactory elemental analyses are achieved for the formulation of the products.

### Crystal structure of 1

Single-crystal X-ray diffraction analysis reveals that **1** crystallizes in the triclinic space group *P*-1. The asymmetric unit consists of two crystallographically independent Zn(II) ions, one $\mathbf{H_2L_1^{2-}}$ and two $\mathbf{L_2}$ ligands, one DMF and two $H_2O$ molecules. Two Zn(II) ions form a paddle-wheel SBU with coordination from four carboxylate groups of two different $\mathbf{H_2L_1^{2-}}$ ligands. Each Zn(II) ion is coordinated by four oxygen atoms of $\mathbf{H_2L_1^{2-}}$ ligands in the equatorial positions, while the axial sites are occupied by the pyridine N atom of $\mathbf{L_2}$, providing a distorted square-pyramidal geometry around the metal. Interestingly, the other pyridine N of $\mathbf{L_2}$ remains uncoordinated (Fig. 1).

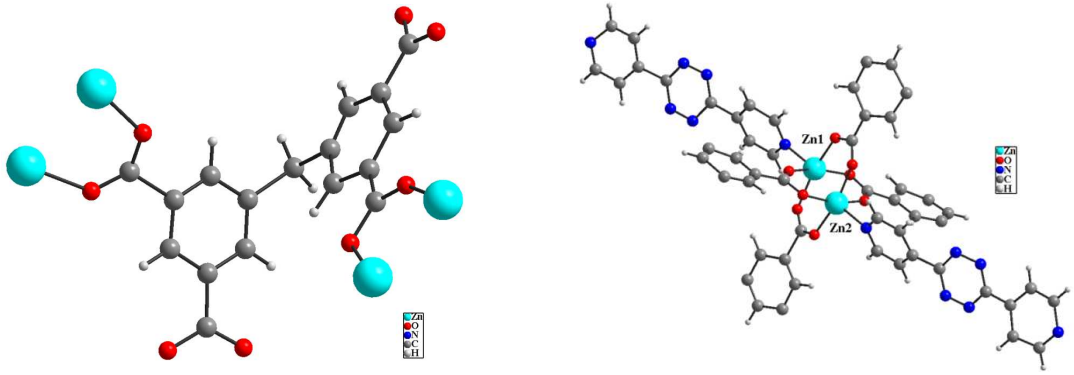


**Fig. 1** Coordination environments of $\mathbf{H_2L_1^{2-}}$ (left) and b) $Zn_2$-paddle wheel unit (right) in **1**.

The ligand $\mathbf{H_2L_1^{2-}}$ exhibits a $\mu_4$-coordination mode in this complex (Fig. 1) and out of four carboxylate groups, only two are coordinated, leaving the other two free. Though, such ligation mode of the bent tetracarboxylate has been realized previously[18], the coordination involving a Zn(II) paddle-wheel building block is unique. Due to the free bond rotation around the methylene group, $\mathbf{H_2L_1^{2-}}$ can adopt either $C_s$ or $C_{2v}$ symmetry[14] (Scheme 1). The ligand $\mathbf{H_2L_1^{2-}}$ shows $C_s$ symmetry in **1**, where two benzene planes are almost perpendicular to each other with a dihedral angle of 86.29° and θ=110.68° at the methylene C atom. This notable kink in $\mathbf{H_2L_1^{2-}}$ provides a platform towards formation of rhombus grids, linked by the $Zn_2(CO_2)_4$ paddle-wheel SBU to form a one-dimensional (1D) double chain. The aromatic planes of $\mathbf{L_2}$ are perpendicular to the planes of the rhomboid-shaped cavities (Fig. 2c), and each repeated 1D double chain is connected along the *c* direction by hydrogen bonding between the tetrazine moiety and the aromatic rings of $\mathbf{H_2L_1^{2-}}$ (*vide infra*). Although the rhomboid cavity is amenable to interpenetration, here it is hindered by the long $\mathbf{L_2}$ ligands, present at the nodes of the square-grid structure.

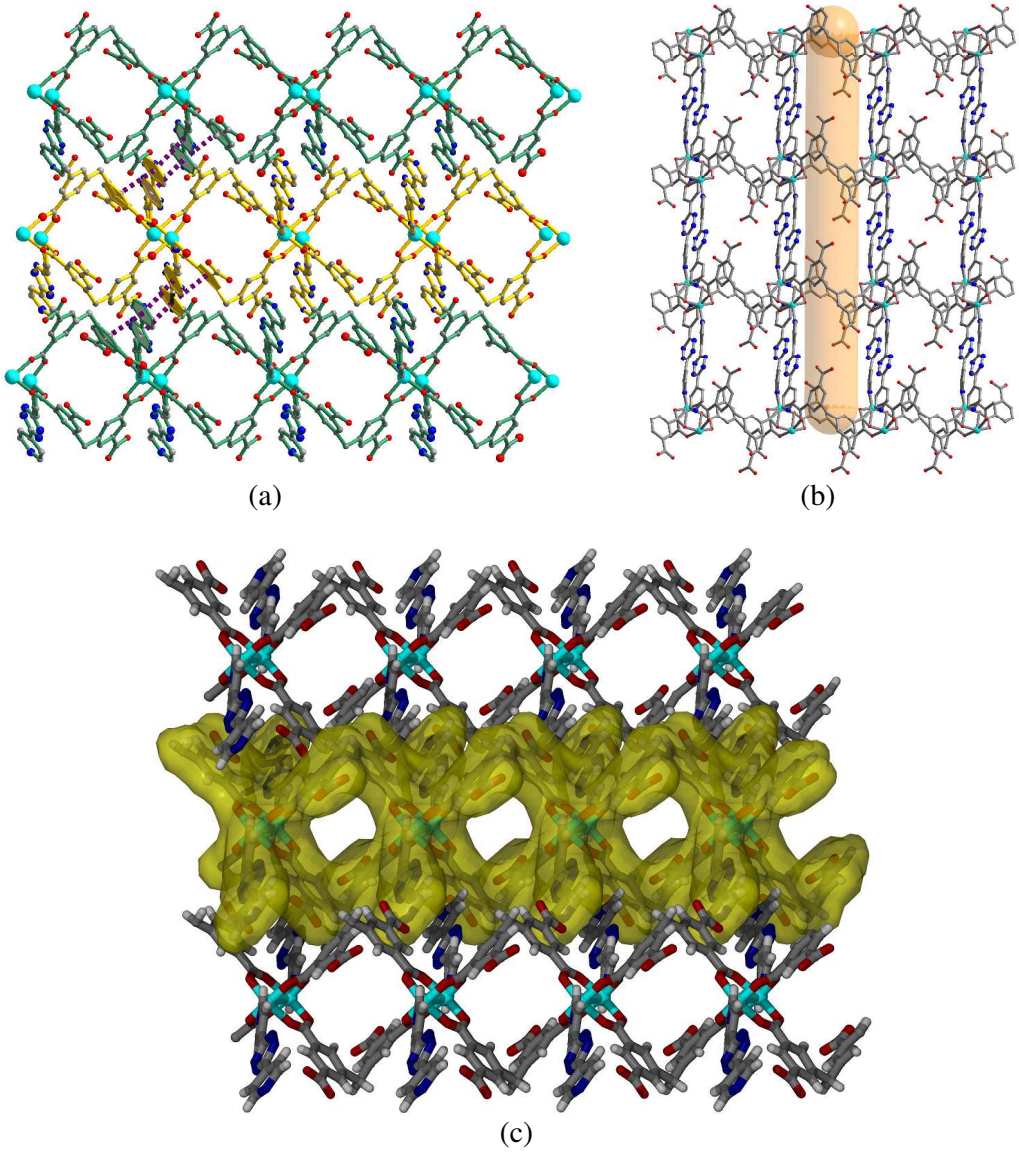


**Fig. 2** 3D packing views of **1** along (a) *c* and (b) *b*-axis, showing free carboxylic acid, pyridine and tetrazene moiety decorated channel. (c) View of the rhomboid cavity along *c*-axis.

These 1D double chains are arranged in sideways as well as above and below each other. The uncoordinated pyridine ends of $\mathbf{L_2}$ are aligned in a head to tail fashion between the first and the neighboring layers, where the molecules assemble into stacks and each molecule has two offset π-stacked interactions with the neighboring molecule. The observed interactions are between relatively electron-poor tetrazine rings and electron-rich pyridine end group, with the distance in the range, 3.47-3.76 Å between the centroids. Another strong π–π stacking (3.41-3.66 Å) exists

between the benzene ring of the carboxylate ligand of one chain and free pyridine end of the neighboring chain (Fig. 2a). The 1D double chain structures are interlinked to each other via these secondary interactions to form an infinite 2D framework. The 2D framework is a porous structure and forms 1D channel along the *c* axis (Fig. 2b). Considering the van der Waals radii of constituting atoms, the maximum channel dimension turns out to be ~6.2 × 4.4 $Å^2$. Another interesting feature of the structure is that the free carboxylate acid groups of $\mathbf{H_2L_1^{-2}}$ as well as tetrazine and pyridine moieties of ligand $\mathbf{L_2}$ are exposed along the channels of the framework. This makes the pore environment both polar and electron deficient, enhancing possible adsorption ability of $CO_2$.

**Crystal structure of 2**

Encouraged by the successful formation of **1**, we decided to replace $\mathbf{L_2}$ by a ligand of comparable length ($\mathbf{L_3}$) and see the change of the resulting complex and pore environment. Swapping the pyridine linker indeed causes a big difference, as revealed by the X-ray crystal structure analysis. The complex (**2**) crystallizes in the orthorhombic space group *Pnma* with the asymmetric unit containing one Zn(II) ion, half of $\mathbf{L_1^{4-}}$, half of $\mathbf{L_3}$ ligand, one metal bound DMF and disordered solvent molecules in the lattice. Here, the Zn(II) ion exhibits penta-coordination with ligation from two carboxylate groups from two different $\mathbf{L_1^{4-}}$, one in chelating and the other in monodendate modes, and a pyridyl N atom from $\mathbf{L_3}$. The fifth coordination site is occupied by a solvent DMF molecule. Unlike **1**, all the carboxylic acid groups of ligand $\mathbf{H_4L_1}$ are deprotonated and bound to Zn(II) ions. Here, the carboxylate ligand adopts a $C_{2v}$ symmetry (Scheme 1), where two phenyl rings face each other forming an angle of 110.68° at the methylene C atom (Fig. 3). When viewed along the *c* axis, the framework exhibits two different types of pores (~ 17.2 × 7.5 $Å^2$ and 10.8 × 8.9 $Å^2$) (the pore size is measured by considering the van der Waals radii of opposite atoms). A close inspection of the layer structure reveals (Fig. 4a)

that the larger pore encompasses ligands $\mathbf{L_1}^{4-}$, $\mathbf{L_3}$ and four Zn(II) ions, while the smaller pore is built from $\mathbf{L_1}^{4-}$ and two Zn(II) ions. Due to the bent nature of this ligand, the layer structure looks like corrugated sheet along crystallographic *a*-axis (Fig. 4c).

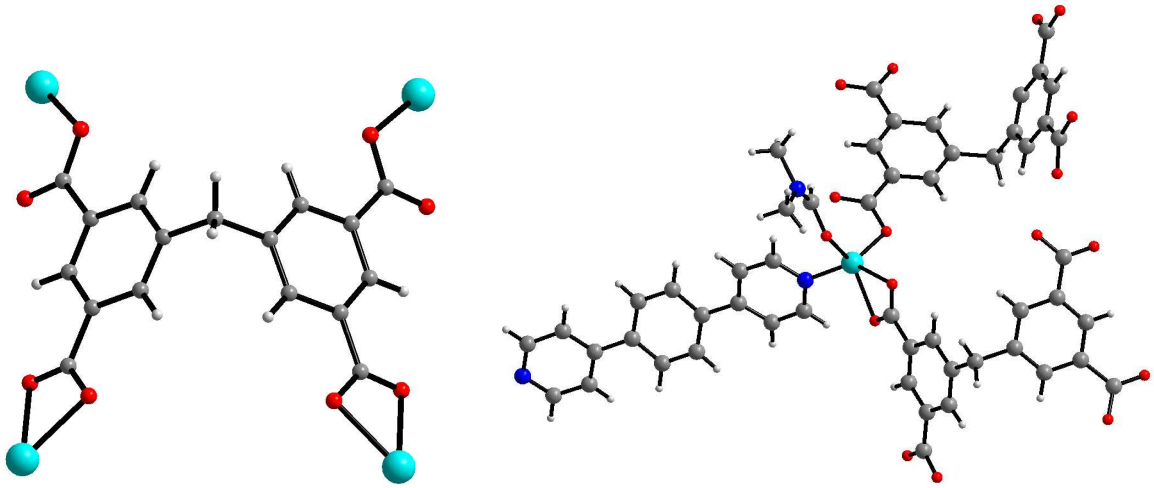

**Fig. 3** Coordination environments of ligand $\mathbf{L_1}^{4-}$ (left) and Zn(II) ion (right) in **2.** (Color code: Zn, cyan; carbon, grey; oxygen, red; nitrogen, blue; hydrogen, white).

The one dimensional sheets are stacked in ---ABAB--- pattern along the crystallographic *b*-axis, with an interplanar spacing of ~4.5 Å, in such a way that two Zn(II) ions of the smaller metallacyclic array are positioned approximately in the middle of the larger pore of the neighboring array (Fig. 4a). The Zn(II) bound DMF molecules are locked inside the larger macrocyclic cavity of the next layer by C–H…π (arene) interaction (2.652 Å & 3.341 Å) between methyl H atom of DMF molecules and the pyridine ring of $\mathbf{L_3}$ (Fig. 4b). It is noteworthy that such locking of DMF solvents to the neighbouring layer completely blocks the pore of the framework. A different C–H…π (arene) interaction (2.707 Å) is evidenced between the methylene H atom of $\mathbf{L_1}^{4-}$ and central benzene ring of the spacer $\mathbf{L_3}$. These secondary forces hold the 2D layer structures and facilitate to pack the sheet structure into a 3D array.

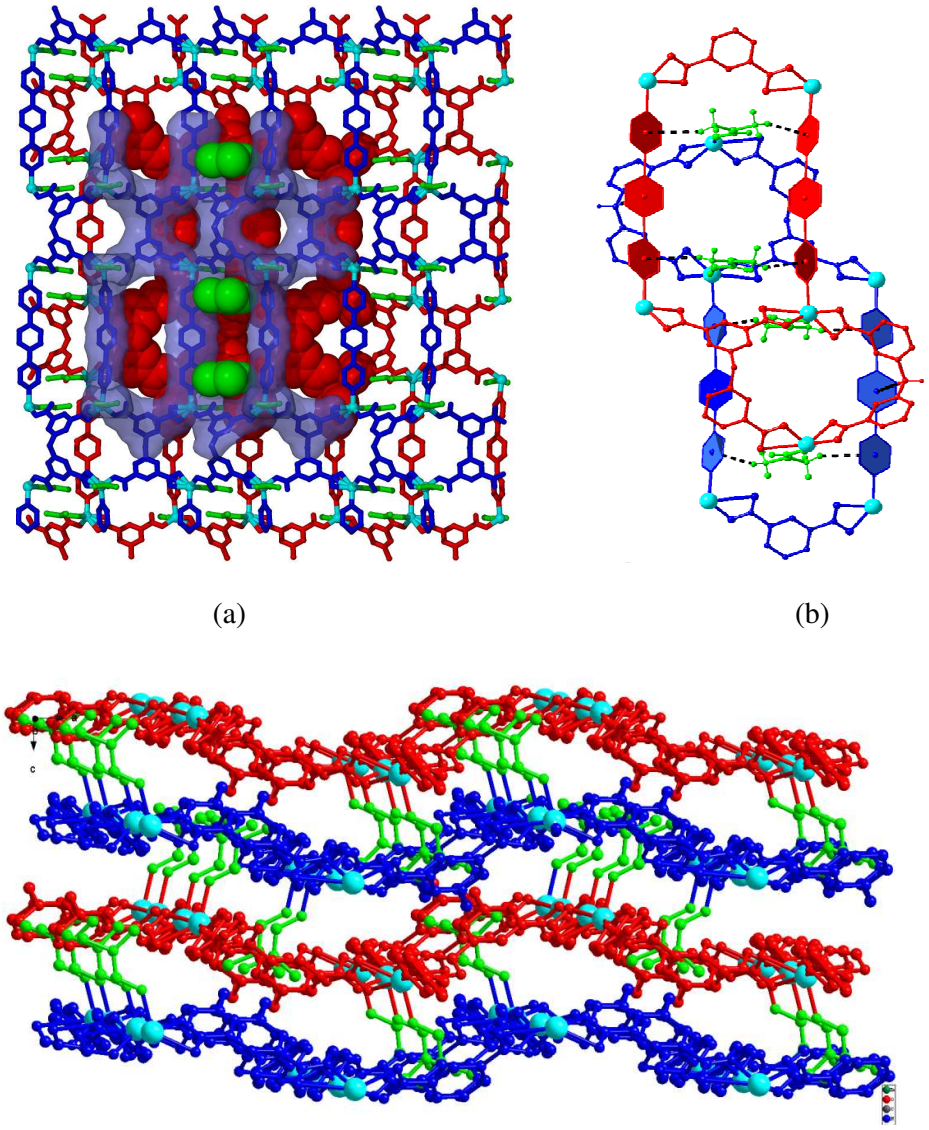

**Fig. 4** (a) Stacking pattern of two adjacent layers (in red and blue) and different sized pores along crystallographic *c*-axis, (b) different C–H–π interactions (in dotted lines) between neighbouring layers, and (c) presentation of ---ABA--- pattern of the 2D sheet in **2**. The solvent DMF molecules, locked inside the larger pores of neighboring layer, are shown in green color. All H-atoms are omitted for clarity.

### Stabilities of 1 and 2

As already stated above, the cavities of both the frameworks are occupied by disordered solvent molecules. PLATON[17] analysis revealed that the 2D structure in **1** contains voids of 475.7 Å$^3$,

representing 28.4% void per unit cell volume, and **2** contains voids of 1059.1 Å$^3$, representing 23.9% void per unit cell volume. Thermogravimetric analysis of **1** shows a weight loss of 14.7 % in the temperature range, 25–130 °C (calcd 14.51 %), corresponding to the complete loss of lattice solvent molecules (Fig. S10†). Thereafter, the TG curve remains unchanged up to 270 °C, above which the linked ligands begin to decompose. The desolvated phase (**1′**) is generated by heating the compound for 16 h at 150 °C under reduced pressure. TGA data confirm the complete removal of guest DMF and $H_2O$ molecules (Fig. S11†). As depicted in Fig. 5, the experimental PXRD patterns of as synthesized **1** are in good agreement with the simulated pattern. Further, the VT-PXRD data indicate that the overall framework integrity **1** are retained at temperature at least up to 200 °C (Fig. 5).

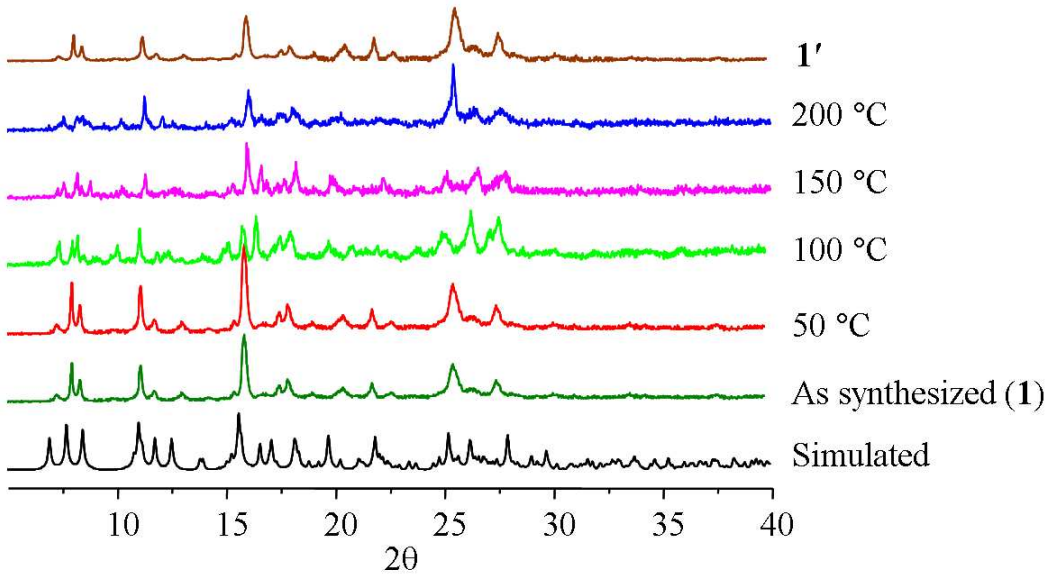


**Fig. 5** Temperature-variable powder X-ray diffraction profile of **1**, together with the powder pattern of the desolvated compound (**1′**).

In contrast to **1**, compound **2** is thermally unstable. Thermogravimetric curve shows that **2** starts loosing solvent molecules at room temperature itself (Fig. S13†). This is also reflected in the inconsistency (Fig. S14†) between simulated and as synthesized PXRD patterns of **2**. Loss of

coordinated DMF molecules at higher temperature leads to complete rupture of the framework. This observation is in line with PXRD of the desolvated framework, where complete loss of crystallinity occurs above 120 °C. We speculate that the H-bonding interactions between coordinated solvent DMF molecule and the framework no longer exist in the desolvated complex, which leads to collapse of the framework.

**Gas adsorption studies**

The porous character of framework **1′**, together with its robust nature and available surface functionalized 1D channel, satisfies the essential pre-requisites for gas sorption measurements. To this end, gas adsorption studies were conducted up to the relative pressure ($p/p_0$) of 1.0 bar on the desolvated complex. Prior to gas adsorption measurements, compound **1** was immersed in ethanol solvent for 3 days at room temperature to replace lattice guest molecules. It was then heated to 120 °C for 12 h under vacuum to produce the guest-free framework (**1′**). The PXRD of **1′** is found to be similar to that of **1** as well as **1** heated at 200° C (Fig. 5). The $CO_2$ adsorption experiment showed a typical type I adsorption behaviour (Fig. 6) at 273 and 298 K, confirming the microporous character of **1′**. The desolvated compound starts to take up $CO_2$ gradually from the low-pressure region. The maximum $CO_2$ uptakes (1 bar) at 273 and 298 K for **1′** are 52.1 and 38.5 $cm^3\ g^{-1}$, respectively. It is noteworthy that the present $CO_2$ sorption results are comparable with the values observed for well-known MOFs like ZIF-9, ZIF- 100, other porous materials like zeolites and activated carbon.[19] Furthermore, it is comparable to MOFs affording pore wall functionalized by acylamide or amide groups, and MOFs decorated by coordination-unsaturated metal sites.[11,20] Nevertheless, the amount of adsorbed $CO_2$ is essentially not comparable to the best values. In order to have more insight on the interaction of the framework with the adsorbate, the isosteric heat of $CO_2$ adsorption ($Q_{st}$) of **1′** is evaluated utilizing the Clausius–Clayperon equation,[21] from the isotherms obtained at 273 and 298 K. As revealed in Fig. 7, the $Q_{st}$ value for

$CO_2$ reaches 21.3 kJ $mol^{-1}$ at high coverage. The relatively low-medium value signifies that although the material exhibits free COOH or pyridine functionalities, this feature seems not to be remarkably important for $CO_2$ adsorption. However, this study gives us a starting point to probe different aspects of porous structures for optimum $CO_2$ adsorption properties. Additionally, the nearly identical $Q_{st}$ values at zero coverage as well as high coverage, together with the obvious plateau (Fig. 7) imply the robustness of the framework.

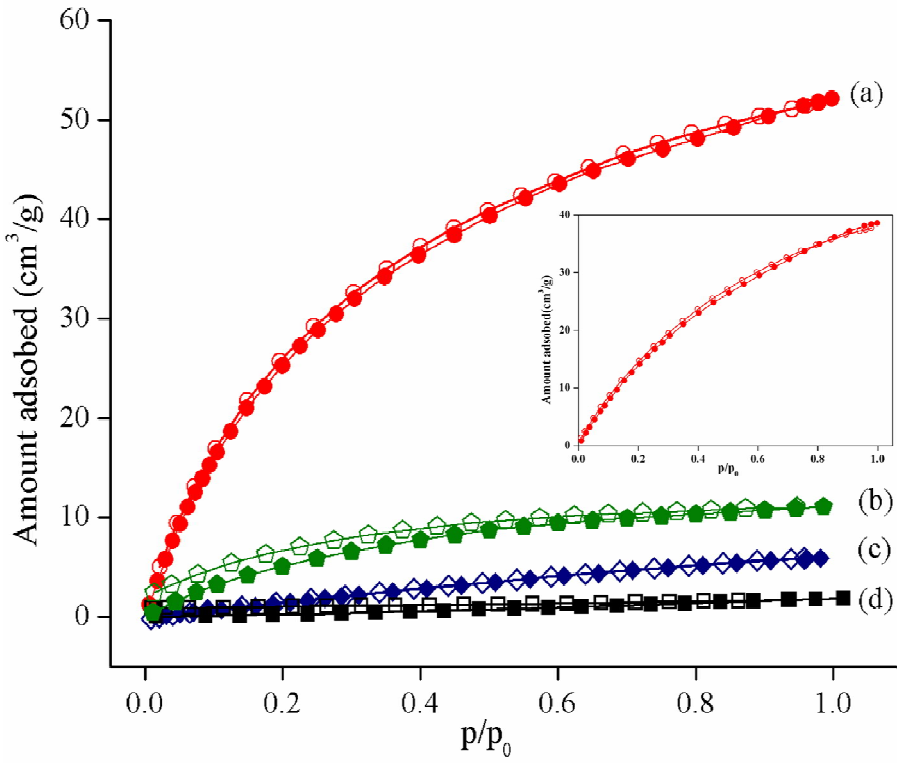


**Fig. 6** Sorption isotherms at 273 K for **1′**: (a) $CO_2$, (b) $CH_4$, (c) $N_2$, and (d) $H_2$ (Adsorption: filled symbol, desorption: empty symbol). Inset: $CO_2$ adsorption isotherm at 298 K.

To further explore the potential properties of **1′** on gas separation under ambient conditions, adsorption isotherms for $H_2$, $CH_4$, and $N_2$ are probed at 273 K. As shown in Fig. 6, $N_2$, $CH_4$ and $H_2$ do not diffuse into the pores of **1′**. Even at 77 K, $N_2$ molecules do not

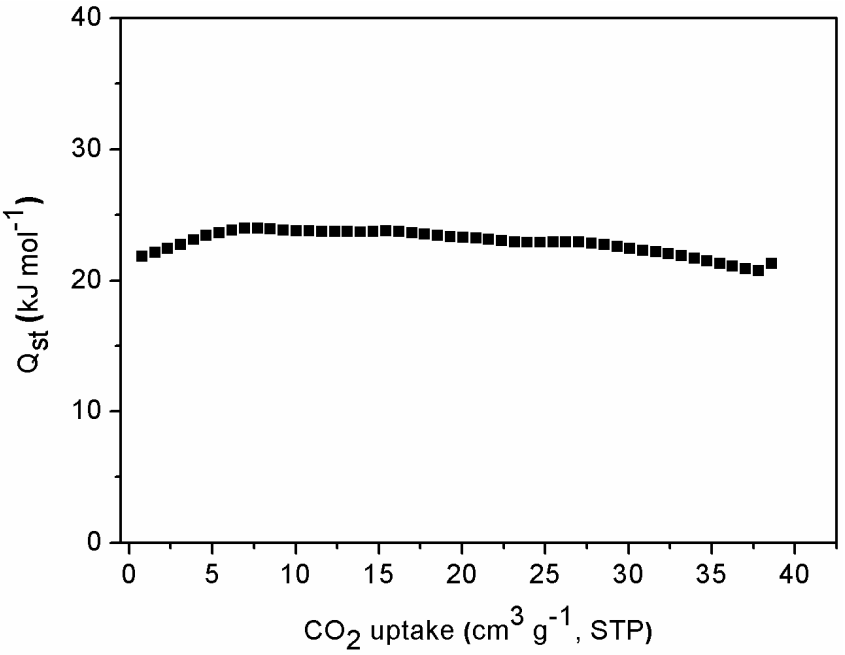


**Fig. 7** Isosteric heat of $CO_2$ adsorption ($Q_{st}$) for **1′**.

diffuse into the channels and only surface adsorption occurs (Fig. S15†). The lack of $N_2$ adsorption at 77 k might be a consequence of its low kinetic energy. Although, the channel size (~6.2 × 4.4 Å$^2$) of **1** is large enough compared to the kinetic diameter of $H_2$ and $N_2$ (2.9 and 3.6 Å, respectively), the insignificant sorption may also be attributed to the fact that 1D channel systems are only available along crystallographic *c*-axis in the framework with no additional effective channels existing along the *a*- or *b*-axes.[19] At very low temperature (77 K), $N_2$ or $H_2$ molecules possibly interact strongly with pore aperture and prevents the next incoming guest molecules to enter into the pore, leading to surface adsorption only. The $CH_4$ molecules, being non-dipolar and non-quadrupolar interact less strongly with the framework. In sharp contrast, the high quadrupole moment and polarizability of $CO_2$ ($13.4 \times 10^{-40}$ C m$^2$ and $26.3 \times 10^{-25}$ cm$^3$, respectively)[22] induce better interaction with the channels and interior wall of the framework, composed of basic tetrazine and pyridine functionalities. The $CO_2$ uptake value at 1 bar (52.1

$cm^3 \cdot g^{-1}$) and 273 K is much higher than those of $H_2$ (1.9 $cm^3 \cdot g^{-1}$), $N_2$ (5.94 $cm^3 \cdot g^{-1}$), and $CH_4$ (11.04 $cm^3 \cdot g^{-1}$).

The significant challenge regarding gas separation under ambient conditions, plus the favorable distinguishing adsorption behavior of the material prompted us to examine the selective $CO_2$ capture ability of **1′** over $N_2$, $H_2$, and $CH_4$ gases at 273 K. The selectivity (S) for adsorption of $CO_2$ over other gases is calculated from the single-component isotherm data. For $CO_2$ capture, this value typically reports the ratio of the adsorbed amount of $CO_2$ at 0.15 bar to the adsorbed amount of other gases at 0.75 bar; the value is normalized for the pressures chosen, according to equation: $S = (q_{CO_2}/q_o)/(p_{CO_2}/p_o)$[23], where $q$ is the amount adsorbed and $p$ is the relative pressure (o = other gases).

The $CO_2$ selectivity over $N_2$, $H_2$ and $CH_4$ are found to be 22, 83 and 11 respectively. Compound **1′** exhibits better $CO_2/N_2$ selectivity compared to other reported MOFs,[11a] suggesting that it may have potential applications in the separation of $CO_2$ from $CO_2$ and $N_2$ mixture. At 273 K, the $CO_2/CH_4$ selectivity for **1′** is however, moderate and comparable to some polyimide networks or ZIFs.[24] Since the critical temperature of $CH_4$ ($T_c$= 191 K) is higher than that of $N_2$ ($T_c$= 126 K),[25] and the gas solubility coefficient is positively correlated with its critical temperature[24a], for **1′**, compared to $N_2$, $CH_4$ has stronger adsorption ability with the framework. As a consequence, $CO_2/CH_4$ selectivity is considerably lower than $CO_2/N_2$.

## Conclusion

The present study demonstrates that an apparent kink in the central methylene spacer of tetracarboxylic acid $\mathbf{H_4L_1}$ can induce either $C_{2v}$ or $C_s$ symmetry in the ligand, which ultimately dictates the overall structure of the resulting framework, in presence of Zn(II) ion and pyridine based linkers of comparable lengths. Thus, in presence of $\mathbf{L_2}$, the carboxylic acid ligand adopt $C_s$ orientation to form a 2D framework **1**, with paddle-wheel $Zn_2(CO_2)_4$ SBU. The strong π…π

interaction between the electron rich and electron deficient parts of aromatic rings from different ligand units extends the 2D framework to the third dimension. Interestingly, porous channel in **1** are decorated with free -COOH and pyridine groups. In contrast, combination of $\mathbf{L_3}$, carboxylic acid ligand and Zn(II) ion results in an extended and corrugated 2D sheet structure **2**, where ligand $\mathbf{L_1}$ assumes a $C_{2v}$ orientation. The 2D sheets comprise of two different voids, which are blocked by Zn(II) ions of neighbouring layers. Thermal stabilities of both the frameworks divulge that **1** is thermally robust towards loss of solvent guest molecules, but **2** readily decompose to amorphous material upon desolvation. Low pressure gas adsorption experiments on desolvated framework (**1′**) at 273 K reveals significant uptake of $CO_2$ and negligible adsorption of $N_2$, $H_2$ and $CH_4$ gases. The dehydrated framework also exhibits good selectivity of $CO_2/N_2$ at 273 K, rendering the framework suitable for gas separation and selective $CO_2$ capture from flue gas. Given the fundamental importance to the interaction between adsorbed $CO_2$ gas and functional organic sites on the pore wall in MOFs, the present study provides a starting point to probe different aspects of porous structures for selective $CO_2$ adsorption. We are presently working along these lines.

## Acknowledgements

We gratefully acknowledge the financial support from the Department of Science and Technology, New Delhi, India (to PKB and SS). SN thanks IIT Kanpur for a postdoctoral fellowship. AA and QX are thankful to AIST for financial support.

## Notes and references

[a]Department of Chemistry, Indian Institute of Technology, Kanpur 208016, India. E-mail: pkb@iitk.ac.in. Fax: (+91) 512-259-7637; Tel: (+91) 512-259-7034.

[b]National Institute of Advanced Industrial Science and Technology (AIST), Ikeda, Osaka 563-8577, Japan. E-mail: q.xu@aist.go.jp. Fax: (+81) 72-751-7942; Tel: (+81) 72-751-9562.

†Electronic supplementary information (ESI) available: Several spectroscopic, thermogravimetric analysis, powder X-Ray diffraction of compound **1** and **2**. X-ray crystallographic data for **1** and **2** in CIF format are provided. CCDC 967622, 967623. For ESI and crystallographic data in CIF or other electronic format see DOI: 10.1039/b000000

1 (*a*) Y. Yan, I. Telepene, S. Yang, X. Lin, W. Kockelmann, A. Dailly, A. J. Blake, W. Lewis, S. G. Walker, D. R. Allan, Barnett, N. R. Champness and M. Schroder, *J. Am. Chem. Soc*., 2010, **132**, 4092; (*b*) S. S. Kaye, A. Dailly, O. M. Yaghi and J. R. Long, *J. Am. Chem. Soc*., 2007, **129**, 14176; (*c*) X. Zhao, B. Xiao, A. J. Fletcher, K. M. Thomas, D. Bradshaw and M. J. Rosseinsky, *Science*, 2004, **306**, 1012.

2 (*a*) A. K. Bar, R. Chakrabarty, G. Mostafa and P. S. Mukherjee, *Angew. Chem., Int. Ed.,* 2008, **47**, 8455; (*b*) T. K. Maji and S. Kitagawa, *Pure Appl. Chem.*, 2007, **79**, 2155; (*c*) M. J. Rosseinsky, *Micropor. Mesopor. Mater.*, 2004, **73**, 15; (*d*) S. Mukherjee, B. Gole, R. Chakraborty and P. S. Mukherjee, *Inorg. Chem.*, 2010, **49**, 10658.

3 (*a*) Y. E. Cheon and M. P. Suh, *Chem. Commun.*, 2009, 2296; (*b*) P. Kanoo, R. Matsuda, M. Higuchi, S. Kitagawa and T. K. Maji, *Chem. Mater.*, 2009, **21**, 5860.

4 (*a*) M. E. Kosal, J.-H. Chou, S. R. Wilson and K. S. Suslick, *Nat. Mater.*, 2002, **1**, 118; (*b*) M. Kondo, T. Okubo, A. Asami, S.-I. Noro, T. Yoshitomi, S. Kitagawa, T. Ishii, H. Matsuzaka and K. Seki, *Angew. Chem., Int. Ed.*, 1999, **38**, 140.

5 (*a*) M. Fujita, Y. J. Kwon, S. Washizu and K. Ogura, *J. Am. Chem. Soc.*, 1994, **116**, 1151; (*b*) C. D. Wu, A. Hu, L. Zhang and W. Lin, *J. Am. Chem. Soc.*, 2005, **127**, 89401; (*c*) B. G. Lor, E. G. Puebla, M. Iglesias, M. A. Monge, C. R. Valero and N. Snejko, *Chem. Mater.*, 2005, **17**, 2568; (*d*) D. N. Dybtsev, A. L. Nuzhdin, H. Chun, K. P. Bryliakov, E. P. Talsi, V. P. Fedin and K. Kim, *Angew. Chem., Int. Ed.*, 2006, **45**, 916; (*e*) T. Uemura, R. Kitaura, Y. Ohta, M. Nagaoka and S. Kitagawa, *Angew. Chem., Int. Ed.* **2006**, *45*, 4112.

6 (*a*) M. H. Mir, L. L. Koh, G. K. Tan, J. J. Vittal, *Angew. Chem., Int. Ed.*, 2010, **49**, 390; (*b*) M. Zeller, *Inorg. Chem.*, 2008, **47**, 5122; (*c*) J. Lipkowski, In *Inclusion Compounds*. J. L. Atwood, J. E. D. Davies and D. D. MacNicol, Eds.; Academic Press: New York, 1984; Vol. 1, pp 59.

7 (*a*) B. Moulton and M. J. Zaworotko, *Chem. Rev.*, 2001, **101**, 1629; (*b*) C. Janiak, *Dalton Trans.*, 2003, 2781.

8 (*a*) R. Kitaura, G. Onoyama, H. Sakamoto, R. Matsuda, S. Noro and S. Kitagawa, *Angew. Chem., Int. Ed.*, 2004, **43**, 2684; (*b*) B. Chen, F. R. Fronczek and A. W. Maverick, *Inorg. Chem.*, 2004, **43**, 8209; (*c*) P. A. Maggard, B. Yan and J. Luo, *Angew. Chem., Int. Ed.*, 2005, **44**, 2; (*d*) S. H. Cho, B. Ma, S. T. Nguyen, J. T. Hupp and T. E. Albrecht-Schmitt, *Chem.Commun.*, 2006, 2563.

9 (*a*) R. Kitaura, K. Fujimoto, S. Noro, M. Kondo and S. Kitagawa, *Angew. Chem., Int. Ed.*, 2002, **41**, 133; (*b*) R. Custelcean and M. G. Gorbunova, *J. Am. Chem. Soc.*, 2005, **127**, 16362.

10 (*a*) S. R. Caskey, A. G. Wong-Foy and A. J. Matzger, *J. Am. Chem. Soc.*, 2008, **130**, 10870; (*b*) R. Vaidhyanathan, S. S. Iremonger, K. W. Dawson and G. K. H. Shimizu, *Chem. Commun.*, 2009, 5230; (*c*) S. S. Nagarkar, A. K. Chaudhari and S. K. Ghosh, *Inorg. Chem.*, 2012, **51**, 572; (*d*) R. Vaidhyanathan, S. S. Iremonger, G. K. H. Shimizu, P. G. Boyd, S. Alavi and T. K. Woo, *Science*, 2010, **330**, 650; (*e*) Y. Inubushi, S. Horika, T. Fukushima, G. Akiyama, R. Matsuda and S. Kitagawa, *Chem. Commun.*, 2010, **46**, 9229.

11 (*a*) K. Sumida, D. L. Rogow, J. A. Mason, T. M. McDonald, E. D. Bloch, Z. R. Herm, T. Bae and J. R. Long, *Chem. Rev.*, 2012, **112**, 724; (*b*) J.-B. Lin, J.-P. Zhang and X.-M. Chen, *J. Am. Chem. Soc.*, 2010, **132**, 6654. (*c*) J. An, S. J. Geib and Rosi, *J. Am. Chem. Soc.*, 2010, **132**, 38; (*d*) T. M. McDonald, D. M. D'Alessandro, R. Krishna and J. R. Long, *Chem. Sci.*, 2011, **2**, 2022; (*e*) R. Dawson, E. Stockel, J. R. Holst, D. J. Adams and A. I. Cooper, *Energy Environ. Sci.*, 2011, **4**, 4239. (*f*) R. Vaidhyanathan, S. S. Iremonger, G. K. H. Shimizu, P. G. Boyd, S. Alavi, T. K. Woo, *Angew. Chem., Int. Ed.*, 2012, **51**, 1826.

12 (*a*) H. Li, M. Eddaoudi, M. O'Keeffe and O. M. Yaghi, *Nature*, 1999, **402**, 276; (*b*) J. L. C. Rowsell, J. Eckert, O. M. Yaghi, *J. Am. Chem. Soc.*, **2005**, **127**, 14904; (*c*) Y. Liu, J. F. Eubank, A. J. Cairns, J. Eckert, V. C. Kravtsov, R. Luebke and M. Eddaoudi *Angew. Chem., Int. Ed.*, 2007, **46**, 3278; (*d*) S. Surblé, C. Serre, C. Mellot-Draznieks, F. Millange, G. Férey, *Chem. Commun.*, 2006, 284.

13 (*a*) M.-H. Zeng, B. Wang, X.-Y. Wang, W.-X. Zhang, X.-M. Chen and S. Gao, *Inorg. Chem.*, 2006, **45**, 7069; (*b*) B.-Q. Ma, K. L. Mulfort and J. T. Hupp, *Inorg. Chem.*, 2005, 44, 4912; (*c*) B. Chen, C. Liang, J. Yang, D. S. Contreras, Y. L. Clancy, E. B. Lobkovsky, O. M. Yaghi, S. Dai, *Angew. Chem., Int. Ed.*, 2006, **45**, 1390; (*d*) K. L. Mulfort and J. T. Hupp, *J. Am. Chem. Soc.*, 2007, **129**, 9604; (*e*) B. Chen, S. Ma, E. J. Hurtado, E. B. Lobkovsky, H.-C. Zhou,

*Inorg. Chem.*, 2007, **46**, 8490; (*f*) M. Xue, S. Ma, Z. Jin, R. M. Schaffino, G.-S. Zhu, E. B. Lobkovsky, S.-L. Qiu and B. Chen, *Inorg. Chem.*, 2008, **47**, 6825.

14 X.-S. Wang, S. Ma, P. M. Forster, D. Yuan, J. Eckert, J. J. López, B. J. Murphy, J. B. Parise and H. C. Zhou, *Angew. Chem., Int. Ed.*, 2008, **47**, 7263.

15 M. Xue, S. Ma, Z. Jin, R. M. Schaffino, G.-S. Zhu, E. B. Lobkovsky, S.-L. Qiu and B. Chen, *Inorg. Chem.*, 2008, **47**, 6825.

16 (*a*) SAINT+, version 6.02; Bruker AXS: Madison, WI, 1999; (*b*) G. M. Sheldrick, SADABS, Empirical Absorption Correction Program; University of Göttingen: Göttingen, Germany, 1997; (*c*) XPREP, 5.1 ed.; Siemens Industrial Automation Inc.: Madison, WI, 1995; (*d*) G. M. Sheldrick, SHELXTL Reference Manual, version 5.1; Bruker AXS: Madison, WI, 1997; (*e*) G. M. Sheldrick, SHELXL-97, Program for Crystal Structure Refinement; University of Göttingen: Göttingen, Germany, 1997.

17 A. L. Spek, *J. Appl. Crystallogr.* 2003, **36**, 7.

18 X. Duan, Q. Meng, Y. Su, Y. Li, C. Duan, X. Ren and C. Lu, *Chem. Eur. J.*, 2011, **17**, 9936.

19 (*a*) R. Banerjee, A. Phan, B. Wang, C. Knobler, H. Furukawa, M. O'Keeffe and O. M. Yaghi, *Science*, 2008, **319**, 939; (*b*) S. Sircar, T. C. Golden and M. B. Rao, *Carbon*, 1996, **34**, 1.

20 (*a*) J. B. Lin, W. Xue, J. P. Zhang, X. M. Chen, *Chem. Commun.*, 2011, **47**, 926; (*b*) K. C. Stylianou, J. E. Warren, S. Y. Chong, J. Rabone, J. Bacsa, D. Bradshaw and M. J. Rosseinsky, *Chem. Commun.*, 2011, **47**, 3389.

21 S. S. Kaye and J. R. Long, *J. Am. Chem. Soc.*, 2005, **127**, 6506.

22 A. Jarad, J. A. Mason, K. Sumida, Z. R. Herm, R. Krishna and J. R. Long, *Energy Environ. Sci.*, 2011, **4**, 3030.

23 T. M. McDonald, D. M. D'Alessandro, R. Krishna and J. R. Long, *Chem. Sci.*, 2011, **2**, 2022.

24 (*a*) G. Li and Z. Wang, *Macromolecules* 2013, **46**, 3058. (*b*) R. Banerjee, H. Furukawa, D. Britt, C. Knobler, M. O'Keeffe and O. M. Yaghi, *J. Am. Chem. Soc.*, 2009, **131**, 3875.

25 J. Jeans, *An Introduction to the Kinetic Theory of Gases*; Cambridge University Press: London, 1982